Journal of Alloys and Compounds 509 (2011) 8692–8699

Contents lists available at ScienceDirect

Journal of Alloys and Compounds

journal homepage: www.elsevier.com/locate/jallcom

Microstructure, phase transformation and mechanical properties of Ni–Mn–Ga–Y magnetic shape memory alloys

Jiehe Sui [a,*], Xin Zhang [a], Li Gao [b], Wei Cai [a]

[a] National Key Laboratory Precision Hot Processing of Metals, P.O. Box 405, Harbin Institute of Technology, Harbin 150001, China
[b] College of Engineering Science and Technoloy, Shanghai Ocean University, Shanghai 201306, China

ARTICLE INFO

Article history:
Received 28 April 2011
Received in revised form 29 May 2011
Accepted 3 June 2011
Available online 21 June 2011

Keywords:
Ferromagnetic shape memory alloy
Rare earth
Phase transformation
Mechanical properties

ABSTRACT

Influence of rare earth Y addition on the microstructure and phase transitions and mechanical properties of polycrystalline $Ni_{50}Mn_{29}Ga_{21}$ ferromagnetic-shape memory alloy (FSMA) are investigated. It is shown that microstructure of the Ni–Mn–Ga–Y alloys consists of the matrix and the Y-rich phase. The Y-rich phase firstly disperses homogeneously in the matrix with small amounts and then tends to segregate at the grain boundaries with increasing Y substitution for Ga. The Y-rich phase is indexed to $Y(Ni,Mn)_4Ga$ phase with a hexagonal $CaCu_5$ type structure. The structural transition from 5 M to 7 M, and then to non-modulated T martensite appears with the increase of Y content. The martensitic transformation temperature increases remarkably with increasing Y content, whereas the Curie temperature almost keeps unchanged. It is revealed that the appropriate addition of Y significantly enhances the yield strength and improves the ductility of the alloys. The mechanism on the influence of Y content on the improved mechanical properties and martensitic transformation temperature is also discussed.

1. Introduction

During the past few years, considerable attention has been devoted to the Ni–Mn–Ga alloy system due to its large magnetic-field-induced strain (up to 10%) and high response frequency (~kHz), which makes it a potential candidate material for new magnetic actuators [1–5]. However, Ni–Mn–Ga alloys exhibit extreme brittleness in spite of single crystal or polycrystalline, which is the biggest obstacle for practical applications. Recent attempts of Ni–Mn–Ga alloys doped using rare earth elements have shown encouraging results. It is found that a proper addition of rare earth elements in Ni–Mn–Ga alloys, such as Tb, Sm or Nd, can improve the ductility of the alloys [6–8]. However, the addition of Sm in $Ni_{48}Mn_{33}Ga_{19}$ alloy decreases the martensitic transformation temperature [7], and the martensitic transformation temperature of Ni–Mn–Ga alloys containing Nd or Tb has a small increase [8,9]. Our recent work reveals that the bending strength and the ductility of $Ni_{50}Mn_{29}Ga_{21}$ alloy are obviously improved with the appropriate addition of Dy or Gd. Furthermore, an obvious increase of the martensitic transformation temperatures is also observed in present alloys by adding Dy or Gd [10]. However, little information about the addition of the rear earth element Y to Ni–Mn–Ga alloys is reported. The purpose of the present work is to investigate the influence of Y on the microstructure, phase transformation behavior and mechanical properties of polycrystalline $Ni_{50}Mn_{29}Ga_{21}$ alloy.

2. Experimental

Polycrystalline $Ni_{50}Mn_{29}Ga_{21-x}Y_x$ (x = 0, 0.1, 0.5, 1, 2, 5 at.%) alloys were prepared from high-purity elements by melting four times in a non-consumed vacuum arc furnace under an argon atmosphere, and then cast into rods with size of 10 mm in diameter and 75 mm in length. The samples were annealed in vacuum quartz tubes at 800 °C for 24 h, followed by water-quenching. The microstructure of the alloys was examined using a Hitachi S-4700 scanning electron microscope (SEM) equipped with an energy dispersive X-ray spectroscopy (EDS) analysis system. Phase identification was performed in a Rigaku D/max-rB X-ray diffractometer (XRD) with Cu Kα radiation. An FEI TECNAI G^2 20 STWIN 200 kV transmission electron microscope equipped with a double-tilt cooling stage was used for TEM studies at room temperature. The phase transformation temperatures were determined by differential scanning calorimetry (DSC) using a Perkin-Elmer Diamond calorimeter with a heating/cooling rate of 20 °C/min and AC susceptibility. The compression tests were performed at room temperature on a Instron 5569 testing system at a crosshead displacement speed of 0.05 mm/min, and the size of the sample was 3 mm × 3 mm × 5 mm.

3. Results and discussion

Fig. 1 shows the backscattered electron images of $Ni_{50}Mn_{29}Ga_{21-x}Y_x$ (x = 0–5) alloys. It is evident that the addition of Y markedly changes the microstructure of ternary $Ni_{50}Mn_{29}Ga_{21}$ alloy and refines the size of the grain. The $Ni_{50}Mn_{29}Ga_{21}$ alloy exhibits a single phase structure, while the white second phase is observed for all the Y-containing alloys. Because the scattering amplitude of the back scattering electron is proportional to the

* Corresponding author. Tel.: +86 451 86412505; fax: +86 45186418649.
E-mail address: suijiehe@hit.edu.cn (J. Sui).

0925-8388/$ – see front matter © 2011 Elsevier B.V. All rights reserved.
doi:10.1016/j.jallcom.2011.06.013

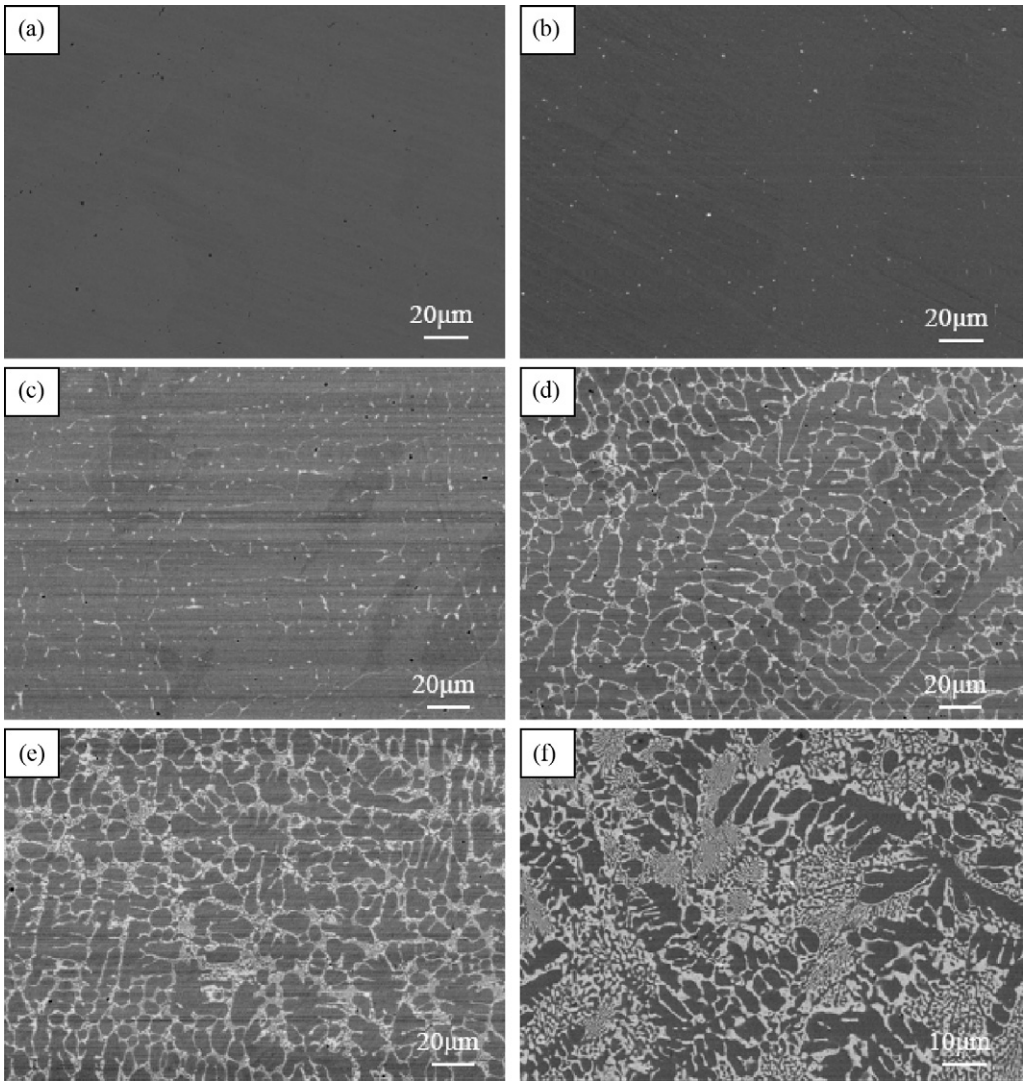

Fig. 1. Backscattered electron images of $Ni_{50}Mn_{29}Ga_{21-x}Y_x$ alloys a) $x = 0$; b) $x = 0.1$; c) $x = 0.5$; d) $x = 1$; e) $x = 2$; f) $x = 5$.

atomic number of the individual element, the content of Y in the white second phase is higher than that in the matrix, indicating the second phase is the Y-rich phase. When the content of Y is 0.1 at.%, small amounts of the Y-rich phase is dispersed in the matrix sporadically. With the increase of Y content, the volume fraction of the Y-rich phase increases gradually, and it tends to distribute along the grain boundaries, as shown in Fig. 1(c)–(e). For the $Ni_{50}Mn_{29}Ga_{19}Y_2$ alloy, the Y-rich phase along the grain boundaries becomes larger and fully connects. Local enrichment of the phase is also found. In particular, the morphology of the $Ni_{50}Mn_{29}Ga_{16}Y_5$ alloy is completely different from that of other alloys, showing a eutectic-like structure. The Y-rich phases are lamellar in the grains, whereas those along the grain boundaries are irregular and have a larger size than those in the grains.

The composition of the matrix and the second phase is listed in Table 1. The EDS results show that the solubility of rare earth Y in the matrix is less than 0.15 at.%, while the solubility in the second phase is high in the range from 15 at.% to 16 at.%. The low solubility of rare earth in the matrix may be attributed to the large atom size of Y. The atom radius of Y is about 1.5 times that of Ni, Mn and Ga atoms. Compared with the compositions of the matrix and the second phase, it can be found that the Ni content of the second phase is slightly higher than that of the matrix, the Ga content has no obvious change, while the Mn content of the matrix is much higher than that of the second phase. It should be noted that the content of Y addition has no obvious effect on the composition of the second phase, while has an obvious influence on the composition of the matrix. With the increase of the Y content, the Mn content of the matrix is increased gradually.

Fig. 2 shows the XRD patterns of as-annealed $Ni_{50}Mn_{29}Ga_{21-x}Y_x$ ($x = 0$, 0.1, 0.5, 1, 2, 5) alloys at room temperature. With

Table 1
The EDS results of $Ni_{50}Mn_{29}Ga_{21-x}Y_x$ alloys (at.%).

Phase	x	Ni	Mn	Ga	Y
The Matrix	0.1	50.46	28.62	20.84	0.08
	0.5	50.02	29.52	20.37	0.09
	1	49.78	30.31	19.78	0.13
	2	49.51	32.03	18.36	0.10
	5	49.87	33.47	16.52	0.14
The second phase	0.1	55.03	8.81	20.68	15.48
	0.5	56.08	8.82	19.72	15.38
	1	59.12	7.28	18.45	15.15
	2	54.58	9.84	20.44	15.14
	5	55.84	9.71	17.89	16.56

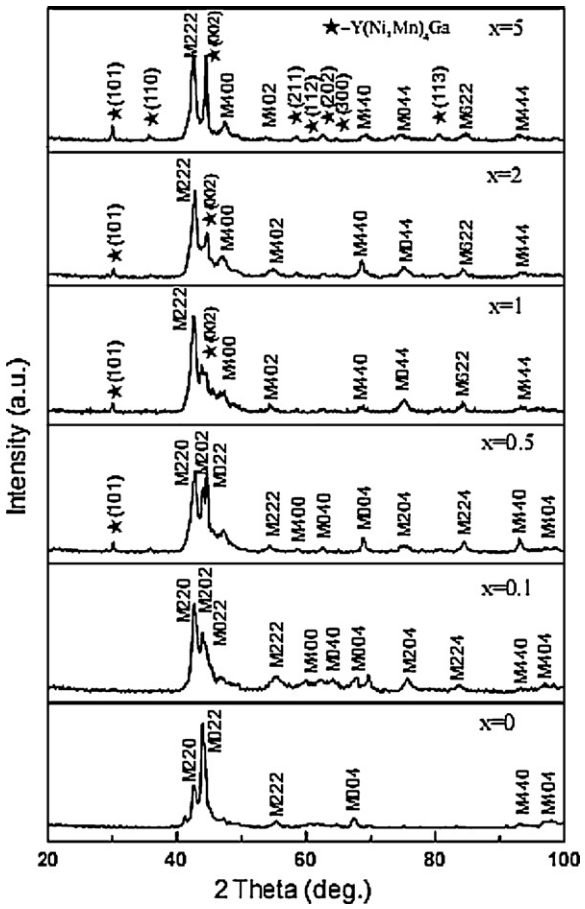

Fig. 2. X-ray diffraction patterns of $Ni_{50}Mn_{29}Ga_{21-x}Y_x$ (x = 0, 0.1, 0.5, 1, 2, 5) alloys at room temperature.

increasing Y substitution for Ga, a different martensitic structure appears. Ternary $Ni_{50}Mn_{29}Ga_{21}$ alloy exhibits a five-layered martensite structure, while the 7 M structures are detected in $Ni_{50}Mn_{29}Ga_{21-x}Y_x$ (x = 0.1, 0.2) alloys and the main reflections are indexed to be orthorhombic structure. For the $Ni_{50}Mn_{29}Ga_{21-x}Y_x$ (x = 1–5), non-modulated T martensitic structure is observed. The lattice parameters and crystal phase for as-annealed $Ni_{50}Mn_{29}Ga_{21-x}Y_x$ alloys are also summarized in Table 2. In order to confirm the martensite structure, transmission electron microscope (TEM) observation was carried out. Two representative electron diffraction patterns (EDP) of the $Ni_{50}Mn_{29}Ga_{20.5}Y_{0.5}$ and $Ni_{50}Mn_{29}Ga_{16}Y_5$ alloys are shown in Fig. 3. The EDP shown in Fig. 3(a) of the $Ni_{50}Mn_{29}Ga_{20.5}Y_{0.5}$ alloy displays six extra superlattice spots between two primary spots, indicating that a seven-layered modulated martensite structure exists. In the same way, however, $Ni_{50}Mn_{29}Ga_{16}Y_5$ alloy is found to be non-modulated T martensite structure, as shown in Fig. 3(b). The TEM results also reveal that the $Ni_{50}Mn_{29}Ga_{20.9}Y_{0.1}$ alloy displays the 7 M structure, whereas the T structures are also observed in both the $Ni_{50}Mn_{29}Ga_{20}Y_1$ and $Ni_{50}Mn_{29}Ga_{19}Y_2$ alloys, which are in good agreement with the results of XRD.

Table 2
The lattice parameters of $Ni_{50}Mn_{29}Ga_{21-x}Y_x$ alloys and the type of the martensitic phase.

Composition	a (nm)	b (nm)	c (nm)	Crystal phase
$Ni_{50}Mn_{29}Ga_{21}$	0.5936	0.5936	0.5537	5 M
$Ni_{50}Mn_{29}Ga_{20.9}Y_{0.1}$	0.6177	0.5838	0.5524	7 M
$Ni_{50}Mn_{29}Ga_{20.5}Y_{0.5}$	0.6253	0.5714	0.5451	7 M
$Ni_{50}Mn_{29}Ga_{20}Y_1$	0.7646	0.7646	0.6797	T
$Ni_{50}Mn_{29}Ga_{19}Y_2$	0.7650	0.7650	0.6761	T
$Ni_{50}Mn_{29}Ga_{16}Y_5$	0.7656	0.7656	0.6839	T

It is worth noting that when x = 0.5 or above for $Ni_{50}Mn_{29}Ga_{21-x}Y_x$ (x = 0, 0.1, 0.5, 1, 2, 5) alloys, in addition to the diffraction peaks of martensite phase, some additional peaks also appear, as indicated by the stars in Fig. 2. The intensity of the additional peaks increases with the increase of the Y content, while their peak positions keep almost constant. This suggests that the new phase may be the Y-rich phase mentioned above as shown in Fig. 1. The XRD pattern of the Y-rich phase is rather similar to that of $SmNi_4Ga$ reported by Devang A. Joshi [11], and the authors think that the XRD pattern of all the RNi_4Ga (R = rare earths) compounds remains the same apart from the position of the lines which will change because the lattice parameters will change. Therefore, all the additional diffraction peaks can be indexed with reference

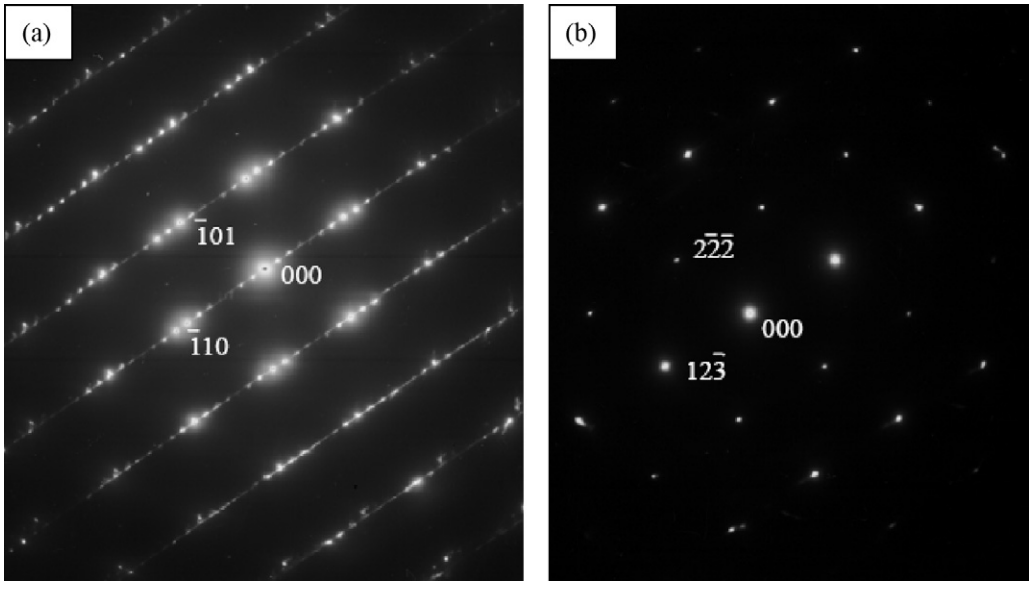

Fig. 3. Electron diffraction patterns at room temperature: (a) $Ni_{50}Mn_{29}Ga_{20.5}Y_{0.5}$ alloy and (b) $Ni_{50}Mn_{29}Ga_{16}Y_5$ alloy.

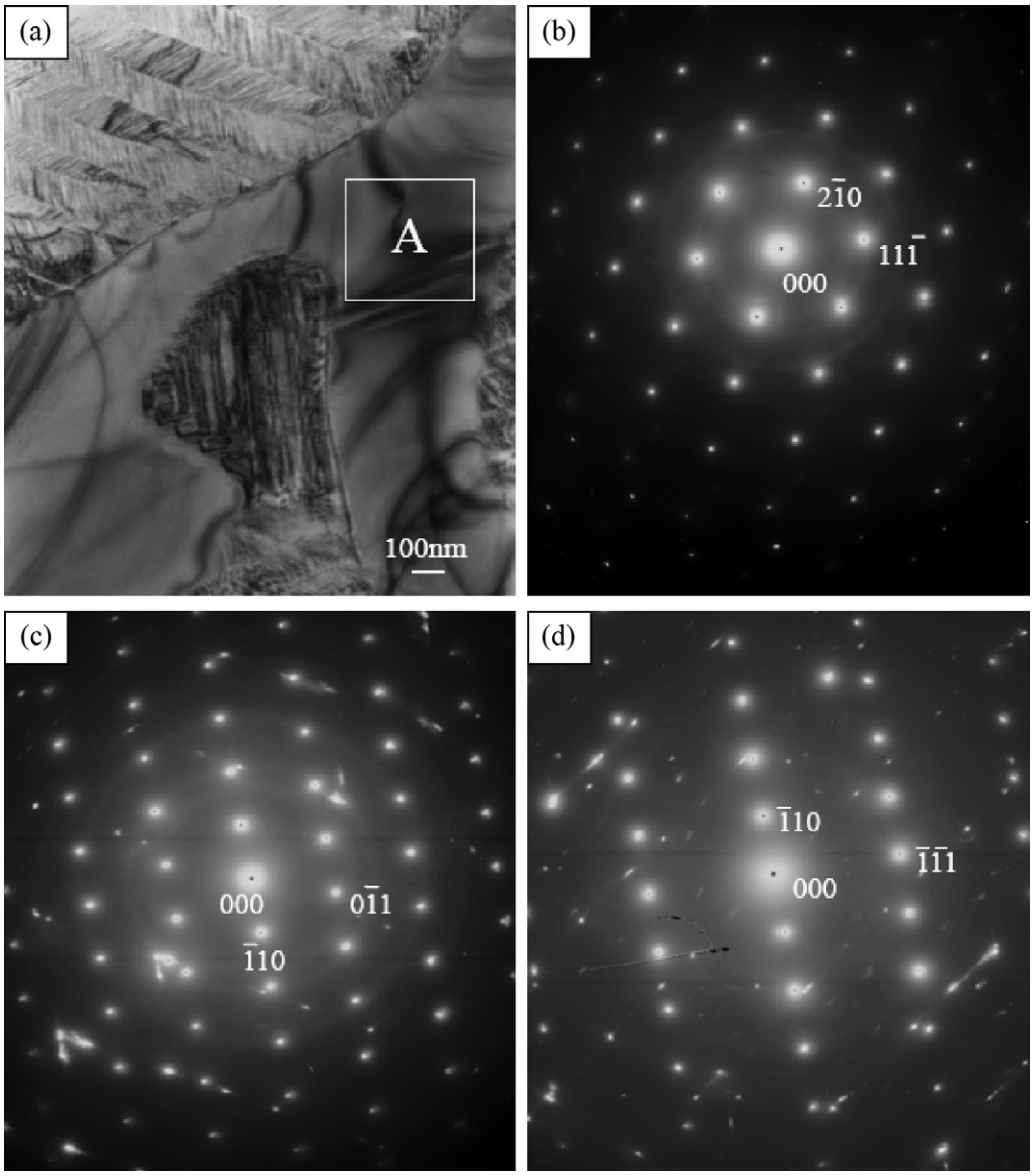

Fig. 4. TEM image of $Ni_{50}Mn_{29}Ga_{16}Y_5$ alloy and the corresponding diffraction patterns. a) Bright field image; b), c) and (d) corresponding EDPs of [1 2 3], [1 1 1] and [1 1 2] zones taken from area A in a), respectively.

to the YNi_4Ga phase. In order to further confirm the structure of the second phase, transmission electron microscope (TEM) observation of the representative $Ni_{50}Mn_{29}Ga_{16}Y_5$ was carried out. Fig. 4a shows a TEM bright field image of the $Ni_{50}Mn_{29}Ga_{16}Y_5$ alloy. It can be seen that the irregular Y-rich phase (area A) is adjacent to the plate-like martensite. Its three SAED patterns, as shown in Fig. 4b–d, can be indexed as $CaCu_5$-type hexagonal structure with the space group of *P*6/*mmm*, which is consistent with the XRD results. The crystal type and space group of the Y-rich phase in the $Ni_{50}Mn_{29}Ga_{16}Y_5$ alloy agree with those of YNi_4Ga. The lattice parameters of this phase are calculated to be $a = b = 0.5018$ nm, $c = 0.4069$ nm, slightly larger than that of YNi_4Ga phase. According to the composition of the second phase listed in Table 1, it can be assumed that the existence of Mn atom in this phase may account for the increase of lattice parameters, and the chemical formula of this phase may be approximately written as $Y(Ni,Mn)_4Ga$. The existence of the $Y(Ni,Mn)_4Ga$ phase in this $Ni_{50}Mn_{29}Ga_{21-x}Y_x$ alloy may have a strong effect on the phase transformation temperatures and the mechanical properties.

Fig. 5 shows the DSC curves for as-annealed $Ni_{50}Mn_{29}Ga_{21-x}Y_x$ alloys. It can be seen that there is only one forward and reverse martensitic transformation during the cooling and heating process, respectively. This indicates that the Ni–Mn–Ga–Y alloys maintain the typical one-step thermoelastic martensitic transformation of the ternary $Ni_{50}Mn_{29}Ga_{21}$ alloy. It can be also clearly seen that the martensitic transformation temperatures increase remarkably with the increase of Y content.

Fig. 6 shows the temperature dependence of AC susceptibility for $Ni_{50}Mn_{29}Ga_{21-x}Y_x$ ($x = 0$, 0.1, 0.5, 1 at.%) alloys. It is well known that two anomalies of AC susceptibility curve are corresponded to the structural and magnetic transitions. It can be seen from Fig. 6(b) that the addition of 0.1 at% Y has no obvious on martensitic transformation temperatures and Curie temperature. When the Y addition is increased to 0.5 at%, an obvious increase of the martensitic transformation temperatures is observed while the Curie temperature almost keeps unchanged as shown in Fig. 6(c). It should be noted that there is a sharp peak in the curve of AC susceptibility during the heating and cooling pro-

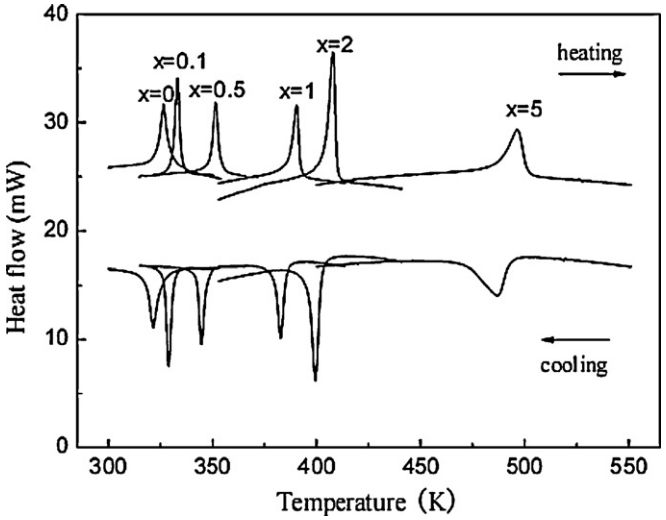

Fig. 5. DSC curves of $Ni_{50}Mn_{29}Ga_{21-x}Y_x$ ($x = 0, 0.1, 0.5, 1, 2, 5$) alloys.

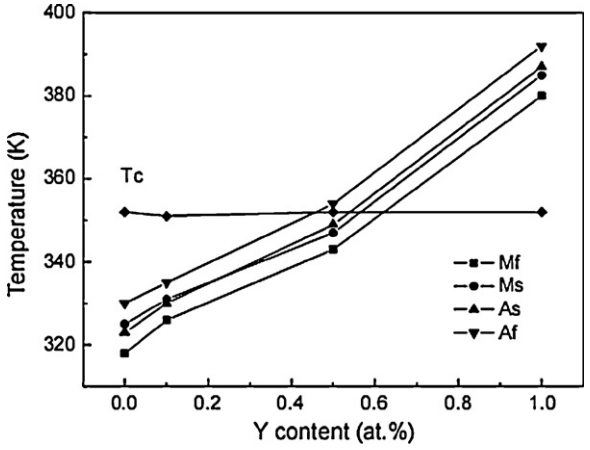

Fig. 7. The transformation temperatures, M_s, M_f, A_s and A_f, and the Curie temperature, Tc, vs.Y content in $Ni_{50}Mn_{29}Ga_{21-x}Y_x$ ($x = 0, 0.1, 0.5, 1$) alloys.

cess. This indicates that the magnetic transition occurs nearly at the reverse martensitic transformation finish temperature. For the $Ni_{50}Mn_{29}Ga_{20}Y_1$ alloy, there is only one abrupt change of the AC susceptibility curve as shown in Fig. 6(d). According to the DSC results, the martensitic transformation of the alloy takes place at 385 K. The temperature of abrupt change consistent with above three Curie temperatures, and the values of susceptibility is very low, therefore, it may be the Curie temperature of the residual austenite phase. It can be concluded that the Curie temperatures of martensite phase is below 270 K which are not observed in Fig. 6.

The Ms, Mf, As, Af and Tc as a function of composition are plotted in Fig. 7 according to the results of DSC shown in Fig. 5 and AC susceptibility measurement shown in Fig. 6. Martensitic transformation temperatures gradually increase while the Curie temperature of austensite keeps almost constant as the Y content increases. With increasing Y content, the curve can be divided into two different regions. When the compositional range of Y is from 0 to 0.5 at%, martensite transformation temperature is lower than the magnetic transition temperature, exhibiting the magnetic transition sequence from paramagnetic martensite to ferromagnetic austenite, and then to paramagnetic austenite. The second region ($x = 1$) is characterized by a high martensitic transformation temperature and a low Curie temperature. In this region, the magnetic transition sequence is from ferromagnetic martensite to paramagnetic martensite, and then to paramagnetic austenite. A martensitic transformation takes place above ferromagnetic

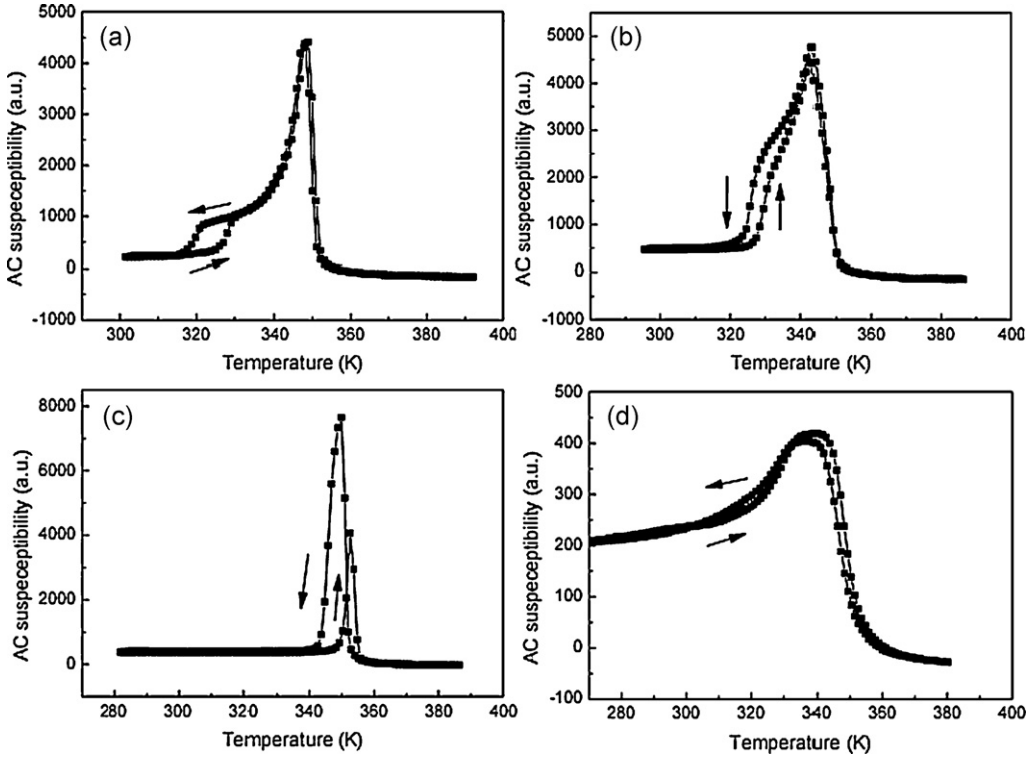

Fig. 6. Temperature dependence of ac susceptibility for $Ni_{50}Mn_{29}Ga_{21-x}Y_x$ alloys with a) $x = 0$, b) $x = 0.1$, c) $x = 0.5$, d) $x = 1$ during the cooling and heating process.

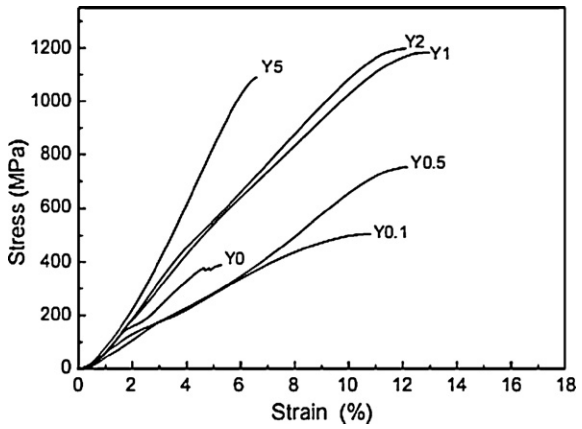

Fig. 8. The compressive stress-strain curves of $Ni_{50}Mn_{29}Ga_{21-x}Y_x$ alloys at room temperature.

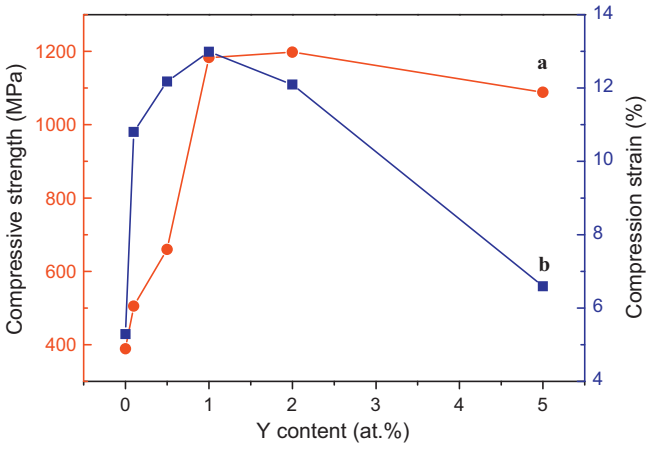

Fig. 9. Effect of Y content on the compressive strength a) and the compressive strain b) of $Ni_{50}Mn_{29}Ga_{21-x}Y_x$ alloys.

transition temperature. The increase of martensitic transformation temperature is closely related to the existence of $Y(Ni,Mn)_4Ga$ precipitate. As mentioned above, $Y(Ni,Mn)_4Ga$ phase contains smaller amounts of Mn compared with the nominal composition of $Ni_{50}Mn_{29}Ga_{21-x}Y_x$ alloys. This implies that the formation of $Y(Ni,Mn)_4Ga$ phase leads to a significant enrichment of Mn in the matrix. Furthermore, the volume fraction of this phase increases gradually with the increase of Y content as shown in Fig. 1. This leads to the continual increase of Mn content in the matrix as listed in Table 1. The solubility of Y in the matrix is less than 0.15 at.% even though in $Ni_{50}Mn_{29}Ga_{16}Y_5$ alloy. Therefore, the change of the Y content in the matrix can be neglected. It is well known that the martenstitic transformation temperatures of Ni–Mn–Ga alloys are very sensitive to the composition of alloys. C.B. Jiang et al. reported that the martensitic transformation temperatures increased monotonically with the increase of Mn content in $Ni_{50}Mn_{25+x}Ga_{25-x}$ alloys [12]. Thus, the change of the matrix composition caused by the presence of $Y(Ni,Mn)_4Ga$ phase results in the increase of the ratio of between Mn and Ga, while keeping the Ni content approximately unchanged, which is responsible for the increase of martensitic transformation temperature. While the Curie temperature has less sensitivity to the composition than the martensitic transformation temperature. Therefore, the Curie temperature keeps constant with trace of rare earth Y element addition.

Fig. 8 shows the compressive stress–strain curves of $Ni_{50}Mn_{29}Ga_{21-x}Y_x$ alloys at room temperature. The compressive strength and strain obtained from Fig. 8 are plotted in Fig. 9. It can be seen that the compressive strength of NiMnGa alloy is obviously enhanced by the Y addition. With the increase in Y content, the compressive strength increases remarkably. The highest compressive strength is obtained in the $Ni_{50}Mn_{28}Ga_{20}Y_1$ alloy (approximately 1180 MPa), which is about 800 MPa higher than that of the alloy without Y addition. Furthermore, it should be noted that the Y addition improves the compressive ductility of the $Ni_{50}Mn_{29}Ga_{21}$ alloy. The compressive strain is increased gradually with increasing Y content and reaches a maximum value in 1 at.% Y-doped alloy. With the further increase in Y content, the compressive strain is decreased largely. This clearly indicates that the proper amount of Y addition significantly improves the compressive strength and the ductility of $Ni_{50}Mn_{29}Ga_{21}$ alloy.

The increase in the strength and strain are mainly due to the refinement of the grains as shown in Fig. 1 and the grain size of $Ni_{50}Mn_{29}Ga_{20}Y_1$ alloy reaches the minimum value. The size and distribution of the Y-rich phase play an important role in affecting the compressive properties of $Ni_{50}Mn_{29}Ga_{21-x}Y_x$ alloys. With the increase in Y content, the Y-rich phase grows and tends to distribute along the grain boundaries. The existence of the Y-rich phase at the grains boundaries effectively hinders the movement of dislocation and the propagation of the cracks, which also plays a positive role in the enhancement of the strength. However, for higher volume of Y-rich phase, the above benefits are offset by the thick network distribution and local enrichment of the Y-rich phase, consequently leading to the decrease in the fracture strength and maximum compressive strain. Thus, the strength and strain reach maximum when $x=1$ and $x=2$, respectively. In addition, rare earth Y distributing along the grain boundaries easily reacts with impurity elements, such as O and S, and restrains the segregation of the impure elements at the grain boundaries. Therefore, the grain boundaries are strengthened because of the reduced damage from impurity elements, which may account for the improvement in the mechanical properties.

In order to clarify the fracture mechanism, the fracture morphologies of $Ni_{50}Mn_{29}Ga_{21-x}Y_x$ alloys after compressing is observed as shown in Fig. 10. It can be seen that from Fig. 10(a) that the fracture type of $Ni_{50}Mn_{29}Ga_{21}$ alloy is the typical intergranular fracture. Compared the fracture morphology with the undoped alloy, the primary fracture type of the $Ni_{50}Mn_{29}Ga_{19.9}Y_{0.1}$ alloy is intergranular fracture. However, transgranular cracks with tearing ridges are also observed. With the further increase of the Y content, the degree of ductile fracture accompanied with tearing ridges of $Ni_{50}Mn_{29}Ga_{21-x}Y_x$ ($x=0.5$, 1) is increased. In particular, lots of dimples with tearing ridges appear in $Ni_{50}Mn_{29}Ga_{20}Y_1$, indicating that the ductile deformation is largely developed before fracture. This accounts for the $Ni_{50}Mn_{29}Ga_{20}Y_1$ alloy possesses the maximum fracture strain. The fracture morphologies change is attribute to strengthening of grain boundary with increasing Y content. When the Y content is increased up to 5 at.%, the fracture morphology with lots of brittle crystal particles is presented. At the same time, the matrix is divided into isolated island by the brittle second phase, further leading to discontinuity of the matrix. Therefore, the crack is easily appeared in the interface between the matrix and the second phase. In summary, the fracture type of Ni–Mn–Ga–Y alloys changes from intergranular fracture to transgranular cleavage fracture with the increase of Y content from 0 to 5 at.% for the $Ni_{50}Mn_{29}Ga_{21-x}Y_x$ alloys. For the $Ni_{50}Mn_{29}Ga_{16}Y_5$ alloy with excessive Y addition, the interphase fracture is observed, which leads to the increase of the brittleness.

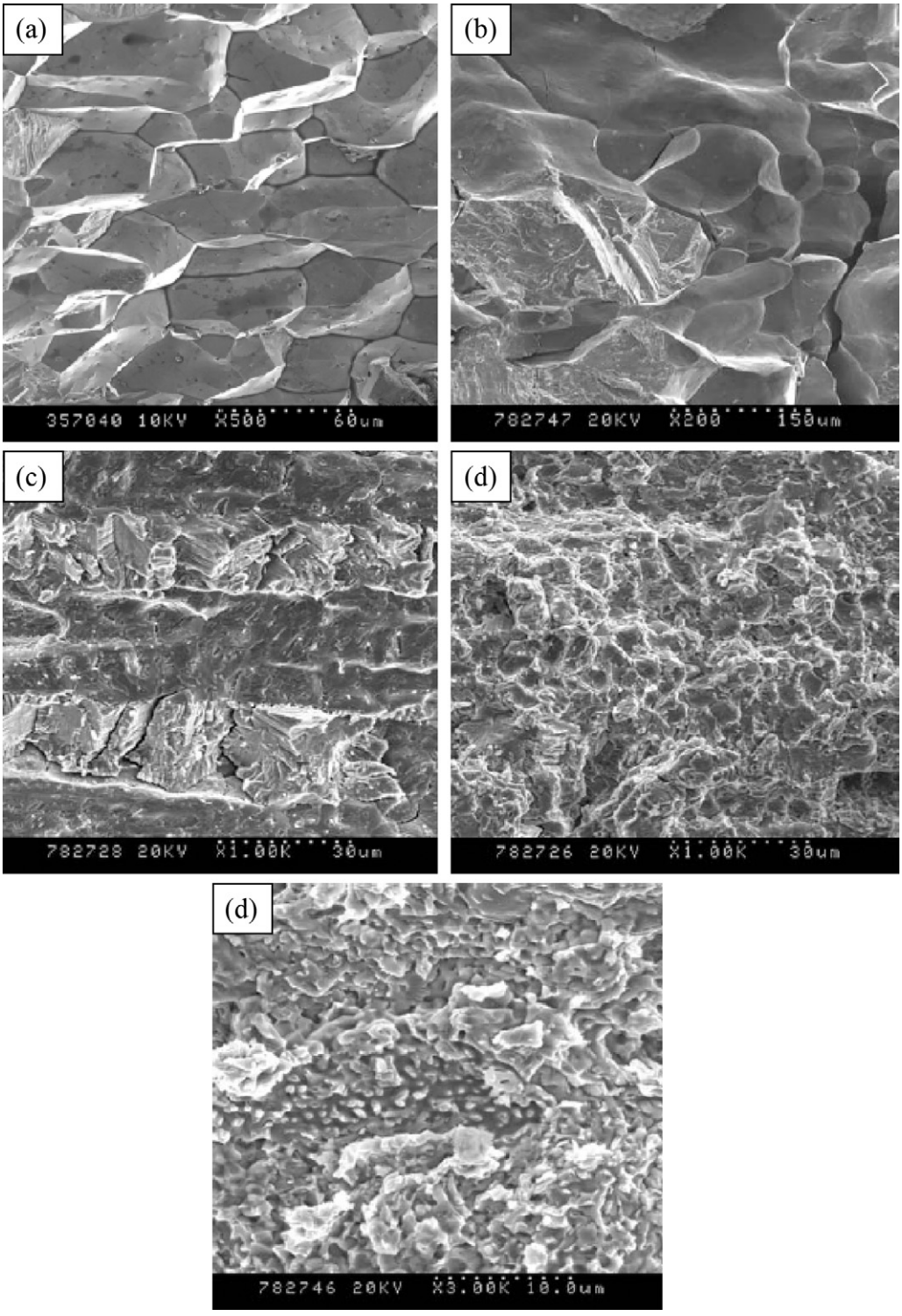

Fig. 10. SEM fractographs of $Ni_{50}Mn_{29}Ga_{21-x}Y_x$ alloys: a) $x = 0$; b) $x = 0.1$; c) $x = 0.5$; d) $x = 1$; e) $x = 5$.

4. Conclusions

The crystal grains of Ni–Mn–Ga–Y alloys can be apparently refined by increasing rare earth content. Ni–Mn–Ga–Y alloys consists of the Ni–Mn–Ga matrix and the hexagonal $Y(Ni,Mn)_4Ga$ phase. With the increase of Y content, the $Y(Ni,Mn)_4Ga$ phase grows and its volume fraction increases gradually. The type of martensites in Ni–Mn–Ga–Y alloys can be modified from 5 M (bct) to 7 M (orthorhombic), and then to non-modulated T martensite (bct) with increasing Y content. Martensitic transformation temperatures of Ni–Mn–Ga–Y alloys notably increase with the increase of Y content, which is mainly due to the increase of Mn content in the matrix caused by the presence of the $Y(Ni,Mn)_4Ga$ precipitate. The Y addition has little influence on the Curie temperature. An appropriate amount of Y addition has significantly improved the mechanical properties of Ni–Mn–Ga alloy, which can be ascribed to the grain refinement. The fracture type changes from intergranular fracture to transgranular cleavage fracture with increasing Y content, which

is due to strengthening of grain boundary with increasing Y content.

Acknowledgment

This work is supported by National Natural Science Foundation of China (no. 50801018).

References

[1] V.A. Chernenko, E. Cesari, V.V. Kokorin, I.N. Vitenko, Scripta Metall. Mater. 33 (1995) 1239.
[2] G.H. Wu, C.H. Yu, L.Q. Meng, J.L. Chen, F.M. Yang, S.R. Qi, W.S. Zhan, Z. Wang, Y.F. Zheng, L.C. Zhao, Appl. Phys. Lett. 75 (1999) 2990.
[3] S.J. Murry, M. Marioni, S.M. Allen, R.C. O'Handley, T.A. Lograsso, Appl. Phys. Lett. 77 (2000) 886.
[4] J. Pons, V.A. Chernenko, R. Santamarta, E. Cesari, Acta Mater. 48 (2000) 3027.
[5] A. Sozinov, A.A. Likhachev, N. Lanska, K. Ullakko, Appl. Phys. Lett. 80 (2002) 1746.
[6] Z.Q. Zhao, W. Xiong, S.X. Wu, X.L. Wang, J. Iron Steel Res. 111 (2004) 55.
[7] S.H. Guo, Y.H. Zhang, Z.Q. Zhao, J.L. Li, X.L. Wang, J. Rare Earths 22 (2004) 632.
[8] K. Tsuchiya, A. Tsutsumi, H. Ohtsuka, M. Umemoto, Mater. Sci. Eng. A 378 (2004) 370.
[9] Z.Q. Zhao, W. Xiong, S.X. Wu, X.L. Wang, J. Rare Earths 22 (2004) 567.
[10] L. Gao, Z.Y. Gao, W. Cai, L.C. Zhao, Mater. Sci. Eng. A 438–440 (2006) 1077.
[11] D.A. Joshi, C.V. Tomy, D.S. Rana, R. Nagarajan, S.K. Malik, Solid State Commun. 137 (2006) 225.
[12] C.B. Jiang, Y. Muhammad, L.F. Deng, W. Wu, H.B. Xu., Acta Mater. 52 (2004) 2779.